Astron. Astrophys. 358, 299–309 (2000)

ASTRONOMY AND ASTROPHYSICS

The kinematical characteristics of the CNM at $\mid b \mid \geq 10^\circ$ and the hypothesis of a local explosive event

W.G.L. Pöppel[⋆] **and P. Marronetti**[⋆⋆]

Instituto Argentino de Radioastronomía, Casilla de Correo 5, 1894 Villa Elisa, B.A., Argentina
(wpoppel@iar.unlp.edu.ar; pedro@galileo.ph.utexas.edu)

Received 11 October 1999 / Accepted 25 February 2000

Abstract. We computed ballistic positions and velocities for test particles, which were ejected a time τ ago, from a small volume at a mean altitude z_0 above the galactic plane at a distance r. The results were fitted to the peaks detected in the residual HI-profiles of observations of the cold neutral medium (CNM) derived from HI-atlases in a former paper. At low latitudes, a significant fraction of the observations is fitted, either by the ballistic model or by Olano's (1982) accretion model for an expanding ring of gas. Another large fraction of the observations corresponds to relatively distant objects, which appear to be mainly in galactic differential rotation. At intermediate and high latitudes the fit by the ballistic model appears to be rather satisfactory for the bulk of the observations. The test particles ejected toward northern altitudes larger than about 72.5° have no observational counterparts but fit an area on the sky, which roughly encloses the well-known northern HI-hole. We suggest that this could be a signature of the explosive event indicating the ionization and transfer of gas into the lower halo.

The fit is less satisfactory for the CNM in the large Sco-Cen shells and the Ori-Eri bubble. Since these regions were affected by star-formation processes *after* the assumed explosive event, we included young disturbance centers in the models, producing isotropic radial accelerations on the affected test particles. This improved the fit significantly. A sample of positions on the high-velocity cloud complex M could be fitted by assuming particles ejected at high velocities with altitudes larger than 77.5°. We conclude that the assumption of an *explosive event* with $\tau = 35\,\mathrm{Myr}$, $z_0 \simeq 35\,\mathrm{pc}$ and $r \simeq 120\,\mathrm{pc}$ in the direction of galactic longitude $l_0 \simeq 140^\circ$, appears to be *consistent* with the observed kinematics of a large deal of the local CNM.

Key words: ISM: clouds – ISM: kinematics and dynamics – Galaxy: solar neighbourhood

1. Introduction

The global characteristics of the interstellar medium (ISM) are very complex. Various phases have been detected. They consist either of neutral gas (cold or warm), or plasma (warm or hot) or a mixture of both. The spatial distributions and filling factors of all the phases are not well known. The morphology of the ISM encompasses filaments, sheets, shells and bubbles of various sizes up to several hundreds of parsecs. Some of the largest objects seem associated to the formation and evolution of OB associations. Cyclic regulating processes, involving galactic fountains, have been proposed for understanding the dynamics and energetics of the ISM (e.g. Ikeuchi 1988, Houck & Bregman 1990).

At *low galactic latitudes* b, on a scale up to about 1 kpc, it is possible to separate two main local HI-features from the very complex galactic background. One is Lindblad's ring or feature A (Lindblad 1967, Lindblad et al. 1973); the other one corresponds to the nearby parts of the local arm (e.g. Sandqvist & Lindroos 1976). Basically, the separation is performed by considering both the radial velocities V and the velocity dispersions σ.

From these two local features the most puzzling seems to be Lindblad's ring, which is closely related to the Gould Belt (GB). This is a flat system of young stars tilted at about 18° to the galactic plane. The kinematics of the GB presents evidences of expansion. Its age should be not larger than about 60 Myr, while its size is of the order of 800 pc (Westin 1985, Lindblad et al. 1997). At least three large nearby OB-associations belong to the GB, namely Ori OB1, Per OB2 and the Sco-Cen association (e.g. Blaauw 1991, de Zeeuw et al. 1999). There are also large molecular cloud complexes associated to the GB and Lindblad's ring (e.g. Dame et al. 1987, Pöppel et al. 1994 [from here on Paper I]).

Two different scenarios have been proposed for understanding the origin of the GB system (i.e. the stars plus the associated gas). One is based on the occurrence of an energetic explosive event (cf. Blaauw 1965, Olano 1982, and Paper I). The other scenario considers collisions of high velocity clouds with the galactic disk (e.g. Franco et al. 1988, Comerón & Torra 1992, 1994, Lépine & Duvert 1994). For further details about the GB system we refer to the review by Pöppel (1997; in the following its Sect. 4.7, which is coauthored with Marronetti & Benaglia, will be called Paper II).

At *intermediate and high latitudes* it is expected that most of the observed HI should be local. In contrast to the case of low

Send offprint requests to: W.G.L. Pöppel

⋆ Member of Carrera del Investigador Científico, CONICET

⋆⋆ now at Center for Relativity, Department of Physics, University of Texas at Austin, Austin, TX 78712, USA

$\mid b \mid$, there is no unambiguous kinematical criterion allowing an assignation to any one of both local features.

The scenario of an explosive event provides us an interesting tool for trying a kinematical identification of some of the local gas at intermediate and high $\mid b \mid$. Already Olano suggested that the HI with $V < 0$, observed toward the galactic poles, should be backfalling remnants of the assumed explosive event. Moreover, in Paper I it was suggested that the well-known large hole in the distribution of the HI with low velocities, which is observed in the northern hemisphere (e.g. Wesselius and Fejes 1973, Kuntz & Danly 1996), should be a signature of this event in the warm neutral medium (WNM).

The cold neutral medium (CNM) detected by means of the 21-cm line appears as the most indicated phase to be analyzed, because: i) its smaller extent in z makes it more susceptible to a local energetic explosion event near the plane than the WNM. Actually, Lindblad's expanding ring is characterized by a narrow σ, and therefore belongs to the CNM; ii) unlike the WNM, the CNM was observed in many directions in absorption (e.g. the optical interstellar lines), as well as in self-absorption. This provides a better chance for deriving distances and making optical identifications; iii) usually, the accuracy of the determination of V is much less sensitive to spurious stray-radiation effects for the narrow features of the CNM than for the broad ones of the WNM (in the case of not too weak components).

In Paper I we made a systematic separation of both the neutral phases in the LISM at $\mid b \mid \geq 10^\circ$ using the atlas of 21-cm profiles of Heiles & Habing (1974) and its southern extension by Colomb et al. (1980), complemented with other data. The velocity range considered was -40 to +40 km s^{-1}. In this paper the kinematical characteristics of the CNM derived in Paper I will be used as an *independent check* of the assumption of a former energetic explosive event in the local interstellar medium (LISM). Briefly, we recall the methods applied in Paper I.

For studying the WNM we sampled the HI-data by means of a mosaic of adjacent cells of $5^\circ \times 4^\circ$ (in galactic coordinates l, b) for $\mid b \mid < 60^\circ$ and of $10^\circ \times 4^\circ$, otherwise. In each cell the emission of the WNM was fitted by one mean broad Gaussian curve ($\sigma \simeq$ 10–14 km s^{-1}). No additional broad components were required.

For studying the CNM we sampled the data from both HI-atlases. By subtracting the mean broad Gaussian curves fitted to the WNM we obtained *residual* profiles. Their *peaks* were assumed to correspond to the CNM. A *statistical analysis* was applied to them for deriving their radial velocities $V_{\rm c}$, equivalent Gaussian velocity dispersions $\sigma_{\rm c}$ and column densities $N_{\rm Hc}$. $V_{\rm c}$ was referred to the local standard of rest (LSR). The distribution of $\sigma_{\rm c}$ peaked at 3 km s^{-1}. For $\mid b \mid \geq 20^\circ$ the mean value was $\overline{\sigma}_{\rm c} \leq 4.5$ km s^{-1}. Clearly, the peaks were *narrow*, as expected of the emission from *cold gas* (e.g. Kulkarni & Heiles 1987). The galactic distributions of $N_{\rm Hc}$ and $V_{\rm c}$ were mapped with a mean sampling of about 1 square degree (cf. Paper I, Figs. 7 and 8, and Paper II, Figs. 4.32–4.37). In the following, we asume that the peaks detected in the residual HI-profiles in Paper I are a significant statistical sampling of the CNM at $\mid b \mid \geq 10^\circ$, and call them the *observed cold clouds* (OCCs).

Our aim is to compare the global kinematics of the OCCs with the computed ballistic positions and radial velocities of massive test particles ejected from an assumed local explosion center. The test particles are moving in the local galactic gravitational field, and we assume that they constitute a sample of the expanding shell produced by the explosive event. In Sect. 2 the results of Paper I for the OCCs are presented on new maps, which are more adequate for our aim. In Sect. 3 we derive ballistic orbits for the test particles. In Sect. 4 we compute the expected positions and velocities of the test particles. We plot them on our new maps of the OCCs for comparison. In Sect. 5 we consider the effects of disturbance centers on the orbits of the test particles. We also consider the large HI-hole, as well as the possibility that some HI-complexes with high and intermediate velocities were originated by the assumed explosive event. Finally, in Sect. 6 we discuss the results and give the conclusions.

2. Kinematics and distribution of the OCCs at $\mid b \mid \geq 10^\circ$

We consider velocities in the range $-40 \leq V_c$ (km s^{-1}) $\leq +40$ and the positions of the OCCs at b-intervals of 10° about each of the following mean values:

$$\overline{b} = +15^\circ, +25^\circ, ..., +85^\circ, -15^\circ, ..., -85^\circ \, .$$

For each b-interval we adopt plane polar diagrams (V, l) for plotting the clouds (in the following we supress the subindex c for simplicity). A scale of colors is used for $N_{\rm H}$. The radial scales are proportional to $cos\ \overline{b}$ as to maintain a constant ratio of pixel to solid angle on the sky. To improve the *statistical significance* of our sample of OCCs we eliminated all those having $N_{\rm H} < 5.2 \times 10^{19}$ cm^{-2}. Such weak objects are more susceptible to observational errors and spurious effects. Moreover, we eliminated a small set of about 2.2% of OCCs having $N_{\rm H} > 104.4$ cm^{-2}. Our final database consists of 13,961 OCCs in the north and 17,188 in the south.

The results are given in Figs. 1–2. For the sake of comparison we also made plots including all the eliminated OCCs (not shown here). A careful comparison with Figs. 1–2 confirmed that the differences were very small and of negligible statistical significance. According to our assumptions in Sect. 1, we consider Figs. 1–2 as a uniform statistical sampling of the CNM over the entire sky at $\mid b \mid \geq 10^\circ$. In the same figures we included the distribution of the high-latitude molecular clouds at $\mid b \mid \geq 25^\circ$ according to the catalogs of Magnani et al. (1996), and Hartmann et al. (1998). The association of this sort of molecular clouds with the cold HI-gas is well apparent in the Figures (cf. Gir et al. 1994). As can be seen from Figs. 1–2, the distribution of the OCCs is rather clumpy. In the following we point out some *general characteristics* of the OCCs.

First, we quote that at $\overline{b} = \pm 15^\circ$ there are numerous OCCs in the galactic quadrants (GQs) II and IV having V in the range -40 to 0 km s^{-1}, as well as in GQs I and III in the range 0 to +40 km s^{-1}. OCCs with $\mid V \mid \geq 10$ km s^{-1} are more loosely clumped. Given their low latitudes, the main velocity contributions of most of this sort of OCCs should stem from the galactic differential rotation. The corresponding rotational distances ex-

tend up to about 2.7 kpc from the Sun. At $\overline{b} = \pm 25°$ this sort of OCCs is less abundant whilst the lower absolute values of their velocities suggest smaller kinematical distances.

Second, we mention two well-known large-scale features, which contain important amounts of cold HI and are expected to be very prominent in our maps, namely i) the loop-like structures or shells surrounding the Sco-Cen association, (de Geus 1992, cf. also Weaver 1979, and Paper II), and ii) the Ori-Eri bubble, (Brown et al. 1994, 1995).

The Sco-Cen HI-shells are seen in the region $l \simeq 240°$ to about $30°$, $b \simeq -50°$ to $+60°$. The main parts are concentrated in the GQ IV. The shells have low velocities and should consist of expanding material swept up by the association from the remnants of the original giant molecular cloud in which the association was formed (de Geus 1988, 1992, Blaauw 1991). We can tentatively identify the cold HI in the Sco-Cen shells in our maps for $\overline{b} = -45°$ to $+65°$, at least. In these maps there is a very dense and clumpy stripe of OCCs with $\mid V \mid < 10\,\mathrm{km\,s^{-1}}$ covering the GQ IV. At $b = -35°$ and $-45°$ the stripe is shorter and presents gaps. At the other latitudes it extends continuously into the GQ III down to about $l \simeq 240°$ without any change of the sign of V. At the higher longitudes the stripe extends continuously into the GQ I, at least up to $l \simeq 20°$ in most of the maps, exceeding somewhat the limits given in de Geus' maps and merging with other OCCs. There is no change of the sign of V at $l = 0°$. Obviously, the persistance of the sign of V at $l = 0°$ and $270°$ suggests the presence of systematic *peculiar motions*.

According to Brown et al. the Ori-Eri bubble could be understood as the product of the winds and supernovae from the Ori OB1 association. The resulting HI-shell is expanding. It extends within the boundaries $l \simeq 165°$–$230°$, $b \simeq -60°$ to $-10°$, with V in the range -40 to $+40\,\mathrm{km\,s^{-1}}$. In our maps for $\overline{b} = -15°$ to $-45°$ we can tentatively identify the most prominent parts of this HI-shell with a very dense and clumpy stripe of OCCs extending along both sides of $l = 180°$. The stripe has positive velocities $\leq +15\,\mathrm{km\,s^{-1}}$ as well as extensions with $V < 0$. It extends down to $l \simeq 160°$, where it merges into a stripe of OCCs with mean velocities $\overline{V} \simeq 0$. At the higher longitudes the stripe ends abruptly near $l \simeq 210°$–$230°$. At $\overline{b} = -55°$ it covers only the range $l \simeq 175°$–$210°$ and has some dense extensions with negative velocities down to $V \simeq -20\,\mathrm{km\,s^{-1}}$. Such extensions exist also at $\overline{b} = -45°$ in the GQ II. Again, $V > 0$ at $l = 180°$ and $V < 0$ in the GQ III are indicating systematic *peculiar motions*.

Third, in the GQ II at $\overline{b} = +35°$ and $+45°$ we quote the presence of some very prominent clumps of OCCs with $V > 0$, indicating *peculiar motions* once more. Most of these clumps should be related to the well-known North Celestial Pole Loop (NCPL), which extends along $l \simeq 120°$–$150°$, and $b \simeq +45°$ down to $+30°$, at least. The region was observed in radio, IR, optical and soft X-rays. It is a candidate for a *collision* between high-velocity gas (from the "string" or "chain A", cf. Hulsbosch 1968) and low-velocity gas (cf. Meyerdierks et al. 1991, Meyerdierks 1992 and the references therein).

Fourth, we consider the latitudes $\mid \overline{b} \mid \geq 45°$ more closely. At $\overline{b} = +45°$ and $+55°$ the velocities of the OCCs are overwhelmingly negative, the main exception being the NCPL at $\overline{b} = +45°$. In contrast, at $\overline{b} = -45°$ and $-55°$ the abundance of OCCs with $V > 0$ is still large. At latitudes $\mid \overline{b} \mid \geq 65°$ the general predominance of $V < 0$ is well apparent. Nevertheless, there are also some faint OCCs with $V > 0$. We quote some remarkable *asymmetries* between both hemispheres:

i) A striking scarcity of OCCs along $l \simeq 70°$–$200°$, at $\overline{b} = +45°, +55°$, and less prominently at $\overline{b} = +65°$. This corresponds to the large northern HI-hole mentioned in Sect. 1.

ii) The presence of some clumps of OCCs with $V < -20\,\mathrm{km\,s^{-1}}$ in the range $l \simeq 90°$–$290°$ at $+55° \leq \overline{b} < +85°$, and over all l at $\overline{b} = +85°$. They correspond to the well-known *intermediate velocity clouds* (IVCs) described by Wesselius and Fejes (1973, cf. Kuntz & Danly 1996, Plate 22). The IVCs overlap partially with the HI-hole. This is consistent with Kulkarni & Fich's (1985) results for the mean HI-profiles observed toward the galactic polar caps. In both cases the profile is centered at *negative* velocities. The northern profile is highly asymmetric with extensions toward about -60 $\mathrm{km\,s^{-1}}$, which are not seen in the southern profile.

iii) A gap in the distribution of the OCCs with low velocities at $l \simeq 225°$–$270°$, for $\overline{b} = -55°, -45°$, with extensions up to $\overline{b} = -15°$. At low latitudes this region overlaps with the elongated cavity of low density found by Frisch & York (1983) from IS line absorption measurements in the UV. Moreover, Ramesh (1994) concluded that at $l \simeq 235°$–$255°$ there is a gap in the distribution of the nearby dark clouds extending up to more than 1 kpc.

iv) Several smaller gaps in the distribution of the OCCs, like those at $\overline{b} = -55°$, $l \simeq 165°$–$175°$, and $300°$–$360°$.

Summarizing, in our maps the OCCs offer a variety of well-defined characteristics regarding their distribution and kinematics. At low latitudes many loosely clumped OCCs appear to be mainly in galactic differential motion. On the other hand, very dense clumpy stripes of OCCs, which present peculiar motions, can be fairly related to prominent large-scale objects, such as the Sco-Cen shells, the Ori-Eri bubble and the NCPL. Moreover, at $\mid \overline{b} \mid \geq 45°$ several galactic north-south asymmetries are apparent in the distribution of the OCCs, as well as an overwhelming predominance of negative velocities.

3. Ballistic orbits for the case of an explosive event

We consider the motions of a group of test particles, which have been ejected simultaneously a time τ ago from a point E located in the galactic plane in the direction of galactic longitude l_0, at a distance r_0 from the Sun. We assume that: i) an energetic explosive event within a dense and massive molecular cloud produced an expanding shell; ii) the braking forces due to the accretion of gas acted drastically in the very initial stages of the event disrupting the cloud and reducing the expansion velocity

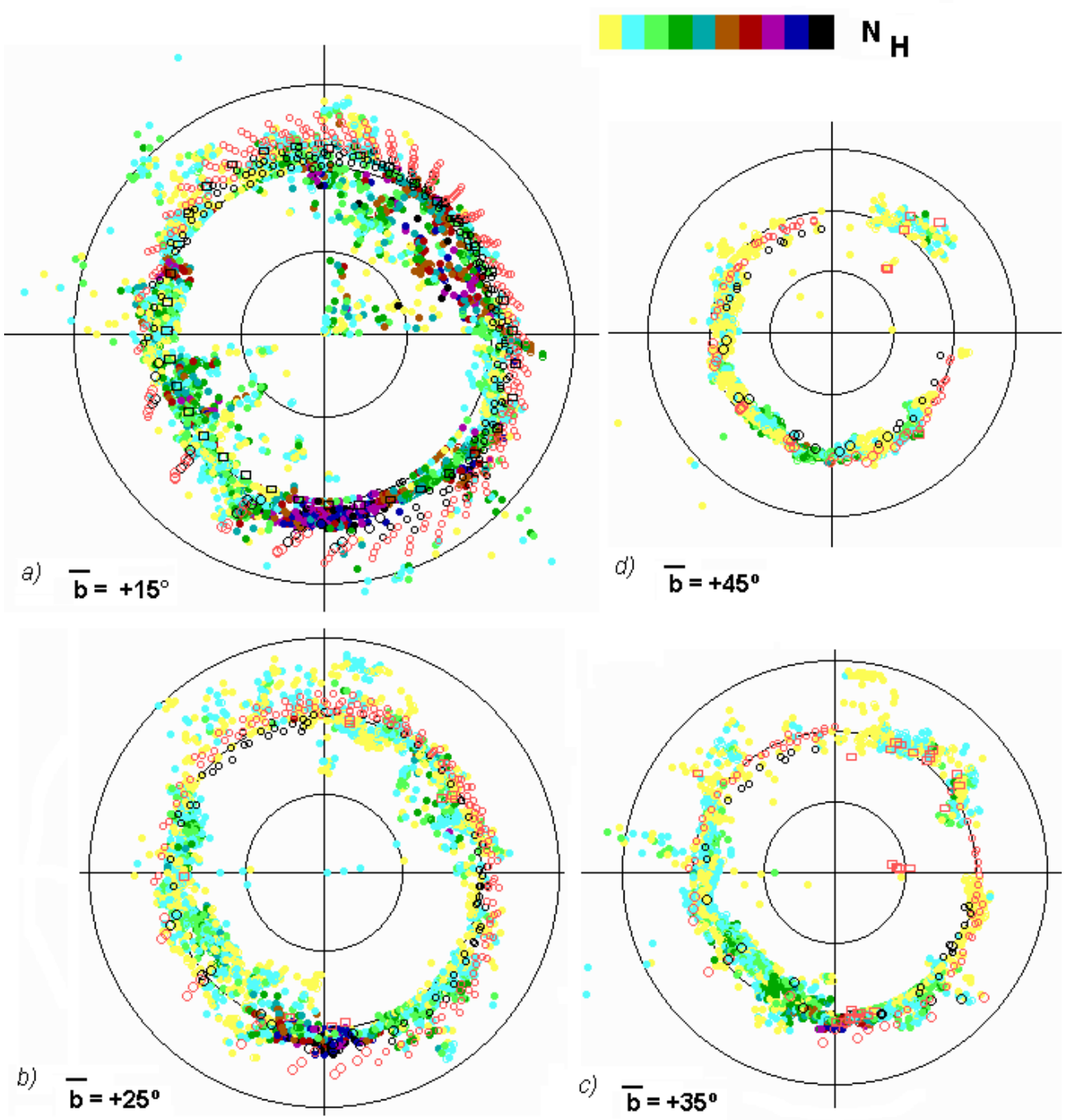

Fig. 1a–d. Polar diagrams for $\bar{b} = +15^\circ$, $+25^\circ$, $+35^\circ$ and $+45^\circ$, showing angular distribution and velocities. Galactic longitudes l increase counterclockwise, $l = 0$ points downwards. The three large concentric circles indicate V(km s^{-1}) = +20, 0 and -20, respectively in order of decreasing radii, whereas -40 is at the center. *Filled circles*: OCCs. The scale of N_H is indicated by means of a wedge of 10 colors. From left to right the following intervals are considered (in units of 10^{19} H at cm^{-2}): 1: 5.2–15.0; 2: 15.1–25.0; 3: 25.1–35.0; 4: 35.1–44.9; 5: 45.0–54.8; 6: 54.9–64.7; 7: 64.8–74.6; 8: 74.7–84.6; 9: 84.7–94.5; 10: 94.6–104.4. *Open black rectangles* (only for $\bar{b} = \pm 15^\circ$): Olano's (1982) model 1. *Open red rectangles* (only for $\mid b \mid \geq 25^\circ$): high-latitude molecular clouds. *Small open circles*: a sample of the test particles fitted by the standard solution (cf. Table 1). The sample is given for $z_0 = 0$ (in red) and $z_0 = 70$ pc (in black), both with $V_0 = 9.5$ and 12.5 km s^{-1}. The interval of α is 10°. The interval of θ is 5° in Figs. 1a–c, and 2.5° in Fig. 1d. *Large open circles*: positions of test particles corrected by the action of asumed disturbance centers. The uncorrected positions were not plotted, except in the case of the Her disturbance center at $l \simeq 45^\circ, b \simeq +35^\circ$.

of a given test particle to an equivalent initial velocity $\boldsymbol{V_0}$; iii) the distances r of the test particles are always small as compared with the distances to the galactic center C; iv) the z-motions can be decoupled from the motions parallel to the galactic plane. These assumptions appear to be adequate for studying the gas

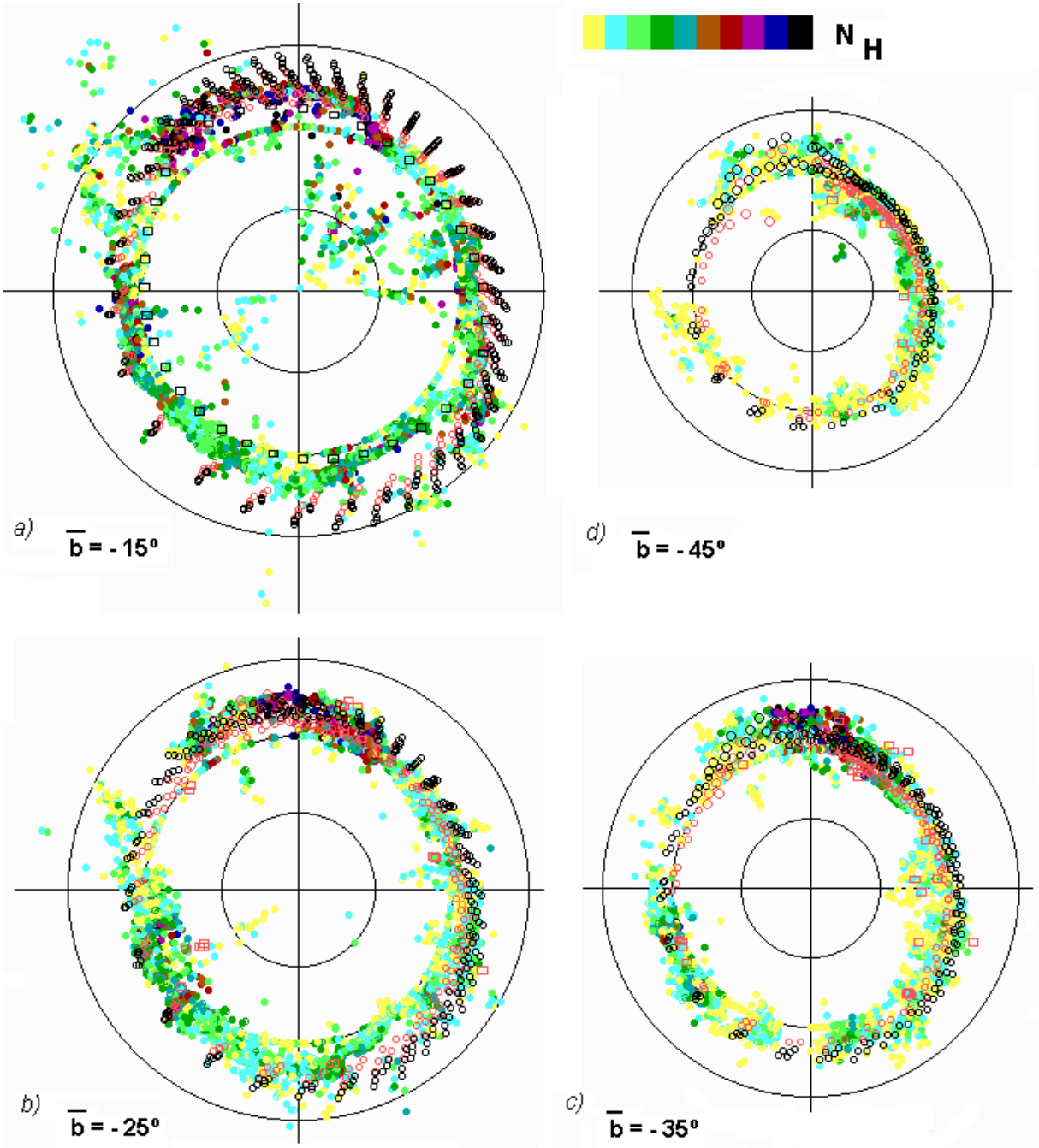

Fig. 2a–d. Same as Figs. 1a–1d for $\bar{b} = -15°$, $-25°$, $-35°$ and $-45°$. The interval of θ used for the sample of test particles is $5°$.

at $\mid b \mid \geq 10°$ since mostly, we avoid the motions near to the galactic plane.

The motions are refered to a system of coordinates ξ, η, z, with its origin at E, which is rotating about C with the angular velocity $\omega_c = 25\,\mathrm{km\,s^{-1}\,kpc^{-1}}$. The ξ-axis points in the direction $l = 180°$, the η-axis in the direction $l = 90°$, and the z-axis in the direction $b = +90°$. Under the assumptions stated above the equations of motion as functions of the time t are well-known (e.g. Olano 1982). If the explosive event is characterized by an isotropic ejection of particles with velocity $\boldsymbol{V_0}$ at $t = 0$, the initial conditions will be

$$\xi(0) = \eta(0) = z(0) = 0\,, \tag{1}$$

$$\begin{aligned} \dot{\xi}(0) &= V_0 cos\theta cos\alpha\,, \dot{\eta}(0) = V_0 cos\theta sin\alpha\,, \\ \dot{z}(0) &= V_0 sin\theta \equiv \dot{z_0}, \end{aligned} \tag{2}$$

where α (azimuth, measured clockwise from the ξ-axis) and θ (altitude, measured northwards from the galactic plane) refer to the direction of ejection.

In this Section we consider that the components F_ξ, F_η and F_z of any interaction force between the ejected test particle and the surrounding medium can be neglected (ballistic orbits).

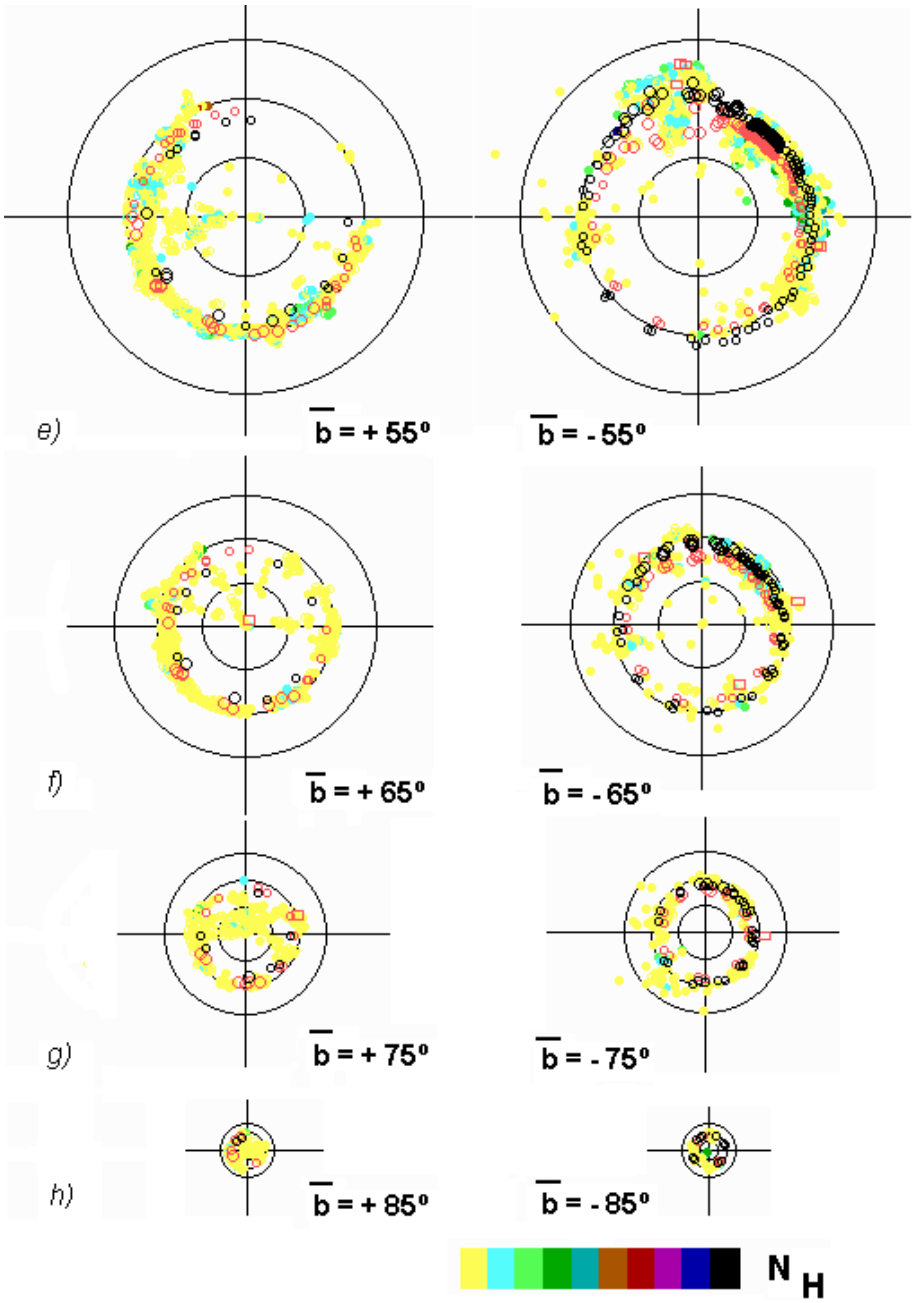

Fig. 1e–h and 2e–h. *Figs. 1e–1h (on the left)*. Same as Figs. 1a–1d for $\bar{b} = +55°$,..., $+85°$. The interval of θ used for the sample of test particles is $2.5°$. *Figs. 2e–2h (on the right)*. Same as Figs. 1a–1d for $\bar{b} = -55°$,..., $-85°$. The interval of θ used for the sample of test particles is $5°$.

Therefore, Chandrasekhar's (1942) analytical solution can be adopted for the ξ- and η-motions, whereas the z-motions can be approximated by small oscillations about the galactic plane with a period T. The latter could become an oversimplification, since the proportionality between the galactic gravitational force per unit mass K_z and the altitude z breaks down at about 350 pc above the plane (cf. Dickey 1993). Nevertheless, small oscillations appear as an acceptable insight into most of the z-motions occurring in our model. We refer to Olano (1982) for further details. In order to allow a comparison with the observations of the CNM, the computed results are referred to an inertial system X, Y, z which we identify with the LSR. If the position and the velocity of the observer are ξ_1, η_1, and $\dot{\xi}_1, \dot{\eta}_1$ respectively, and the observer measures l, b, r, and V, we have:

$$sinb = z/\sqrt{(\xi - \xi_1)^2 + (\eta - \eta_1)^2 + z^2}\,, \tag{3}$$

$$tgl = -(\eta - \eta_1)/(\xi - \xi_1)\,. \tag{4}$$

$$r = \sqrt{(\xi - \xi_1)^2 + (\eta - \eta_1)^2 + z^2}\,, \tag{5}$$

$$V = \dot{z}sinb - \dot{X}coslcosb + \dot{Y}sinlcosb\,. \tag{6}$$

The computations of r can be checked independently of the 21-cm observations in all those cases where identifications of the clouds are possible and the distances are known. Furthermore, in our computations we considered also an initial altitude z_0

Table 1. Adopted parameters for the standard solution

τ; T (Myr)	$35; 100$
$\xi_1, \eta_1; z_\odot$ (pc)	-93, -77; $+15$
z_0 (pc)	0, +35, +70
$\dot{\xi}_1, \dot{\eta}_1, \dot{z}_1$ (km s^{-1})	$+0.6$, -1.5, -1.5
α ($^\circ$)	$0, 5, ..., 355$
θ ($^\circ$)	-90, -87.5, ..., +72.5
V_0 (km s^{-1})	$9.5, 10.5, ..., 12.5$

of E above the galactic plane (cf. Paper I), a velocity $\dot{z}_1$ of the observer, as well as an altitude $z_\odot$ of the Sun above the galactic plane.

4. Computations of the positions and radial velocities of the test particles. Results

4.1. Standard analytical solution for the low velocities

We adopted the value of τ and the position of the observer consistent with Olano's (1982) accretion models. These were derived for $b \simeq 0^\circ$ considering the effect of braking forces in the galactic gas layer. In the following we will consider Olano's model 1 ($\tau = 35$ Myr, $r_0 = 121$ pc, $l_0 = 140^\circ$) and assume $T = 100$ Myr. Tests with $T = 80$ and 120 Myr supplied no adequate fit of the OCCs. All the adopted parameters are listed in Table 1.

We started by assuming an *isotropic* ejection of the test particles ($360^\circ \geq \alpha \geq 0^\circ$, $+90^\circ \geq \theta \geq -90^\circ$), and $z_0 = 35$ pc. The values assumed for V_0 covered an interval of only 3 km s^{-1} in order to be consistent with a shell-like structure. It turned out that the resulting velocity-dispersion of the test particles was smaller than the one of the OCCs by a factor of about 3. Increasing the range of V_0 produced no significant improving since the solutions were not very sensitive to V_0 at intermediate and high latitudes. A variation of z_0 was more effective. An adequate V-dispersion was obtained for the set of values of z_0 given in Table 1. This suggests that our test particles were ejected from a small volume, as is consistent with Blaauw's (1983, 1991) suggestions about the minimum sizes of the initial configurations in OB associations. Furthermore, we adopted $z_\odot = +15$ pc (e.g. Cohen 1995, Ng et al. 1997, Minezaki et al. 1998) and fitted $\dot{z}_1 = -1.5$ km s^{-1}.

As the mean altitude of the explosion center E is $\overline{z}_0 = +35$ pc, our model predicts *asymmetries* between both galactic hemispheres. Since $T/4 < \tau < T/2$, particles ejected northwards ($\theta > 0$) with $V_0 \sin\theta << 2\pi z_0 \mathrm{T}^{-1} \simeq 4$ km s^{-1} will be already in the southern hemisphere shortly after $t = T/4$. As a result, there will be more particles in the south than in the north. This should be reinforced by the effect of $z_\odot > 0$. Moreover, the particles in the south ($z < 0$) will be at earlier phases on their motions back to the galactic plane, than those in the north. On the other hand, a gap in the distribution of the test points in the GQ II at some northern latitudes could be fitted by a *cutoff* at $\theta_0 = +72.5^\circ$.

In the following we describe the results obtained for a *standard solution* with the set of free parameters given in Table 1. For each z_0 we computed the position and radial velocities of 19008 test particles in order to have an adequate coverage in the polar diagrams for a comparison with the OCCs. We considered the same latitude intervals as in Sect. 2. The solutions included the distances of the fitted test particles.

4.2. Comparison of the results of the standard solution with the observations

A representative sample of the results of the standard solution were plotted in Figs. 1–2. In most cases the test points form a stripe extending along the entire range of l, with a thickness between about 4 and 10 km s^{-1}. In the following we make a comparison of the computed test points with the OCCs.

i) The low latitudes $\overline{b} = \pm 15^\circ$ (cf. Figs. 1a and 2a).
Here the predominance of *positive* velocities among the test points is overwhelming, as is expected of an expanding ring, which is observed from the inside. Consequently, the loosely clumped population of OCCs with *negative* velocities down to -40 km s^{-1} in the GQs II and IV are not fitted. Analogously, the loosely clumped OCCs with $V > 20$ km s^{-1} in GQs I and III are not fitted as well. This is consistent with the interpretation that most of these OCCs correspond to more distant objects, which are mainly in differential rotation about the galactic center.

The standard solution fits a large fraction of the dense stripe of OCCs with *low* positive velocities in the GQs II and III. In particular, the fit includes many prominent OCCs with *peculiar* velocities, like those near to $l \simeq 180^\circ$. However, in the GQs I and IV the dense stripe of OCCs has either small *positive* velocities, which are *lower* than the predicted ones, or slightly negative velocities. This suggests that the *braking forces* cannot be neglected. Our standard solution fits only a small fraction of these OCCs. Olano's model 1 predicts *lower* velocities and makes a more successful fitting attempt in GQs I and IV. Actually, it fits the smooth dense stripe with peculiar velocities along $l \simeq 240^\circ$–270° at $\overline{b} = +15^\circ$. The latter should belong to the Sco-Cen shells.

ii) The low latitudes $\overline{b} = \pm 25^\circ$ (cf. Figs. 1b and 2b).
Here the standard solution predicts mostly $V > 0$ as well as some moderately $V < 0$. It fits dense stripes of OCCs in the GQs I (at $\overline{b} = +25^\circ$), II and III, including some with peculiar velocities, like those at $l \simeq 160^\circ$–180°. Nevertheless, the effect of the braking forces appears to be still present in some regions, like in the GQ I at $\overline{b} = -25^\circ$, where the velocities of the broad dense stripes of OCCs are systematically *lower* than the predicted ones. We quote the *peculiar negative velocities* at $l \simeq 245^\circ$–270°, $\overline{b} = +25^\circ$ (belonging to the Sco-Cen shells), and at the spikes at $l \simeq 205^\circ, \overline{b} = -25^\circ$, and $l \simeq 180^\circ$, $\overline{b} = +25^\circ$. On the other hand, at $\overline{b} = +25^\circ$ most of the OCCs with $V \leq -3$ km s^{-1} in GQ II, and $V \geq +6$ km s^{-1}, in the range $l \simeq 180^\circ$–230° at $\overline{b} = +25^\circ$ could correspond to more distant objects moving on circular orbits about the galactic center. Finally, in the GQ IV many of the OCCs of the Sco-Cen

shells have $V < 0$, whereas a smaller group has $V > 0$. They are fitted only marginally by the standard solution.

iii) The intermediate latitudes: $\overline{b} = \pm 35°, \pm 45°$ and $\pm 55°$ (cf. Figs. 1c–1e and 2c–2e).

Here we expect that the OCCs should be mainly *nearby* objects. The predicted values of V are low, either positive or negative. Only in the GQs I and IV at $\overline{b} = -35°$ the predicted velocities are still mainly positive. At the *negative* latitudes the standard solution fits the bulk of the OCCs in the GQs I (somewhat marginally at $\overline{b} = -35°$), II and IV, as well as many OCCs in the GQ III. Among the non-fitted OCCs with $V > 0$ we quote: a) the dense clumps with $V > +2$–$5\,\mathrm{km\,s^{-1}}$ in the region $l \simeq 160°$–$225°$, which should belong to the Ori-Eri bubble; b) some clumps with $V \geq +5\,\mathrm{km\,s^{-1}}$ in the regions $l \simeq 240°$–$280°$, $\overline{b} = -35°$, and $l \simeq 270°$–$300°$, $\overline{b} = -45°$, which should all belong to the Sco-Cen shells; c) several clumps with $V > +8\,\mathrm{km\,s^{-1}}$ in the GQ I. Among the non-fitted OCCs with $V < 0$ the most notorious are some dense clumps having velocities in the range $\simeq -2$ to $-20\,\mathrm{km\,s^{-1}}$, which are concentrated at: a) $l \simeq 150°$–$180°$, $\overline{b} = -35°$ and $-45°$, as well as $l \simeq 185°$–$205°$, $\overline{b} = -55°$ (presumably, all related to the Ori-Eri bubble), and b) the region $l \simeq 60°$–$120°$, $\overline{b} = -35°$ and $-45°$. Some of these OCCs have *peculiar motions*. Furthermore, a few OCCs with $V < -20\,\mathrm{km\,s^{-1}}$ at $\overline{b} = -45°$ and $-55°$ are not fitted as well.

At the *positive* latitudes the predicted velocities are more negative than at $b < 0$. The test particles form a horseshoelike arc along the GQs III, IV and I, which fits the broad bulk of OCCs. In the GQ II, the large gap at $\overline{b} = +45°$ and $+55°$, which is related to the HI-hole, is fitted roughly by the cutoff at θ_0 (cf. Table 1). The non-fitted OCCs in GQ II have mainly $V > 0$ and should be related to the puzzling NCPL mentioned in Sect. 2. Notorious non-fitted clouds with $V > 0$ are the plumes at $\overline{b} = +35°$, $l \simeq 48°$ (Her shell, e.g. Bates et al. 1995), $215°$–$240°$, and $261°$. We point out the densely populated areas of OCCs with $V < 0$, which should be related to the extensive Sco-Cen shells in the GQ IV. They are fitted only marginally at $\overline{b} = +35°$ and $+45°$, and much better at $+55°$. At this latitude we quote also a group of IVCs.

iv) The high latitudes: $\overline{b} = \pm 65°, \pm 75°$ and $\pm 85°$ (cf. Figs. 1f–1h and 2f–2h).

Here the predicted velocities are negative in almost all the cases. The standard solution fits most of the OCCs with $V < 0$ at $b < 0$. At $b > 0$ the fit is rather less complete, because of the presence of the IVCs, most of which are in the range $l \simeq 90°$–$290°$. Moreover, some puzzling non fitted OCCs with $V > 0$, appear mainly in the GQs III and IV at positive and negative latitudes. They could be outlayers of the Sco-Cen shells.

5. Further peculiarities of the observed cold clouds

5.1. Disturbance centers

In the last Section we pointed out several dense groups of clumps of OCCs having peculiar velocities, which are not fitted by the standard solution. Many of these OCCs should belong either to the Sco-Cen shells or to the Ori-Eri bubble. These objects are driven by the associations Sco-Cen and Ori OB1 respectively, which are not older than 15 Myr (Blaauw 1991). This suggests the production of *local changes* in the original densities and velocities of the expanding shell during the formation and evolution of the associations, assuming that they interacted with the shell.

Table 2. Adopted parameters for the disturbance centers

	l_d (°)	b_d (°)	r_d(pc)	t(Myr)	s(pc)	k
Her	45	35	145	0.4	40	0.12
Ori	195	-40	200	6.0	120	1.00
Loop I	330	35	210	4.0	160	0.22
NCPL	135	32	130	5.0	50	1.00

In order to test this possibility, we assumed the appearance of single *isotropic disturbance centers*. A given disturbance center D can arise in the direction l_d, b_d at a distance r_d from the Sun, producing a spherical disturbance of radius s during a time interval t, which is short compared with τ. The force components F_ξ, F_η and F_z will not vanish now. We assumed a solution of the form

$$\xi = \xi_1 + \xi_2, \eta = \eta_1 + \eta_2, z = z_1 + z_2, \tag{7}$$

where the subindex 1 refers to the ballistic solutions while 2 refers to small *corrections* produced by the disturbance center. We considered a test particle located at ξ_1, η_1, z_1 at a distance $s' < s$ from D. A *linear isotropic* mean radial acceleration of magnitude $2ks/t^2$ was assumed to act on the test particle, during a time interval $\Delta t = (1 - s'/s)t$. The intensity parameter k was assumed to be in the range 0–1. Simple solutions ξ_2, η_2 and z_2 were obtained. In this manner, small corrections could be fitted changing the position and the velocity of the test particle.

Three independent disturbance centers were considered, namely in Orion, in Hercules, and at the Loop I center. The adopted parameters are listed in Table 2. The results were plotted in Figs. 1–2 replacing the original test points from the standard solution. In the region of the Ori-Eri bubble the disturbance produced small bumps at $\overline{b} = -35°, -45$ and $-55°$, with a significant improvement of the fit. This was also the case for the spike in Hercules at $\overline{b} = +35°$. The Loop I disturbance acted on the Sco-Cen region improving the fit at $\overline{b} = +25°, +35°$ and $+45°$. We conclude that our results are well consistent with the assumption of significant modifications of the original distribution of the OCCs in Lindblad's ring by the action of the new star formation activity.

5.2. The HI-hole

We have seen that a cutoff at $\theta_0 = 72.5°$ produces a large gap in the distribution of the northern test particles in GQ II. Globally, the gap seems consistent with the large HI-hole mentioned in Sect. 1. To test this more closely, we considered the locus of the test particles ejected at three selected values of $\theta \geq \theta_0$. The adopted parameters were those of our standard solution with

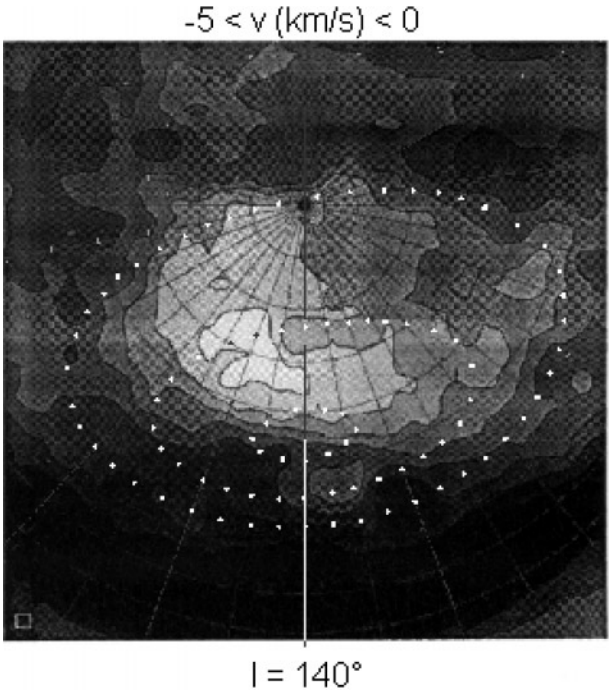

Fig. 3. Locus of the tests particles ejected with $z_0 = 35\,\mathrm{pc}$; $V_0 = 12.5\,\mathrm{km\,s^{-1}}$; $\alpha = 0^\circ$–360°, and the values of θ given in Table 3. The loci are superposed on a contour map derived by Kuntz & Danly (1996) for radial velocities in the range -5 to 0 $\mathrm{km\,s^{-1}}$. The grid correspond to galactic coordinates with a space of 10° in l and b. See the text for more details.

Table 3. Characteristic parameters of the loci of particles ejected with large values of θ, $z_0 = 35\,\mathrm{pc}$ and $V_0 = 12.5\,\mathrm{km\,s^{-1}}$

θ	l_1	b_1	V_1	r_1	z_1	l_2	b_2	V_2	r_2	z_2
(°)	(°)	(°)	$\mathrm{kms^{-1}}$	pc	pc	(°)	(°)	$\mathrm{kms^{-1}}$	pc	pc
72.5	157	24	+1.3	285	116	22	87	−7.1	130	130
80.0	150	31	−1.6	237	122	133	67	−7.4	143	132
87.0	142	40	−4.1	197	127	137	50	−6.0	169	129

$V_0 = 12.5\,\mathrm{km\,s^{-1}}$ and $z_0 = +35\,\mathrm{pc}$ (cf. Table1). The values of θ are shown in Table 3. For each locus we indicate the coordinates l_1, b_1, velocity V_1, distance r_1, and altitude z_1 of the test point having the *lowest* b. Similar quantities are also given for the one having the *highest* b (subindex 2). The three loci are plotted in Fig. 3 superposed on an HI-contour map derived by Kuntz & Danly (1996) for radial velocities in the range -5 to $0\,\mathrm{km\,s^{-1}}$, where the HI-hole is well apparent. As can be seen, each locus forms a loop, the outer one corresponding to $\theta = 72.5^\circ$. It seems to enclose roughly the HI-hole. For each computed locus its top border is nearer to us and has approaching velocities, while the bottom border has receding velocities (cf. Table 3). In contrast, the values of z are similar for both borders. These characteristics are expected for a hole produced by a nearby explosive event, It should be interesting to check them *observationally*. Moreover, Fig. 3 suggests that our standard solution is a simplification in the sense, that the cutoff-values of θ could be a function of α.

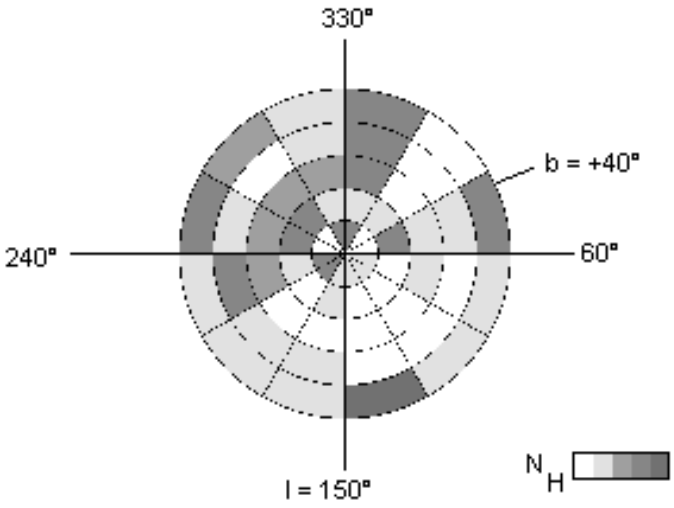

Fig. 4. Distribution of the column densities N_H of the large velocity dispersion component of the ISM at the northern Galactic Pole cap, as derived from Westphalen's (1997) data. The five intervals considered are (in units of 10^{18} H atoms $\mathrm{cm^{-2}}$): 1: 10.0–12.9; 2: 13.0–15.9; 3: 16.0–18.9; 4: 19.0–21.9; 5: 22.0–24.9.

We quote that for $\theta = 72.5^\circ$ the locus encloses only *partially* the large area of the most intense X-ray enhancement detected at high positive latitudes in the ROSAT 1/4 keV band (Snowden et al. 1995, cf. their Fig. 5c). Thus, the large northern X-ray enhancement appears related to two different sources at least. They could be the HI-hole and the North Polar Spur.

Furthermore, it was not possible to fit the gas with $V > 0$ related to the NCPL at $\bar{b} = +35^\circ$ and $+45^\circ$, neither by means of the standard solution nor by varying V_0. Computations for particles ejected *beyond* the cutoff (i.e. with $\theta \geq 72.5^\circ$) produced only *negative* velocities at $\bar{b} = +45^\circ$. Therefore, we computed the effects of an *isotropic disturbance center* acting on test particles, whose initial parameters were

$$\begin{aligned} z_0 &= +35\,\mathrm{pc}\,, \\ V_0 &= 9.5\,\mathrm{km\,s^{-1}}\,, \\ \theta(^\circ) &= +72.5,\ +75.0, ...,\ +90\,, \end{aligned}$$

and else, those of Table 1. The adopted disturbance parameters are shown in Table 2. In these conditions, at $\bar{b} = +35^\circ$ we obtained test particles having positions and velocities qualitatively similar to those of the OCCs related to the NCPL (cf. Fig. 1c).

5.3. High and intermediate velocity complexes

In Paper I it was shown, that the scenario of an explosive event is consistent with large z-extensions of the IS gas, as well as with the observed parameters of some nearby intermediate velocity (IV) and high velocity cloud (HVC) complexes. Therefore, we tried to fit some sample positions of the HVC complex M (Herbstmeier et al. 1995) and the IV cloud bridge (Kuntz & Danly 1996) by means of test particles ejected from E with the general parameters of the standard solution (cf. rows 1–4 of Table 1, with $z_0 = 35\,\mathrm{pc}$), and *particular values* of α, θ and V_0.

Table 4. Adopted parameters for the fit of IV and HVC complexes

	l (°)	b (°)	V kms^{-1}	V_0 kms^{-1}	α (°)	θ (°)	r kpc	z kpc
M I A	167	65	−115	252	70.5	82.0	3.4	3.1
B	155	67	−90	187	82.0	82.5	2.5	2.3
C	145	67	−85	173	92.0	82.5	2.3	2.1
D	138	67	−90	183	99.0	82.0	2.4	2.2
M II A	186	65	−85	185	44.0	83.0	2.5	2.3
B	178	67	−88	184	54.0	83.5	2.4	2.2
M III	182	57	−110	331	54.0	79.0	4.8	4.0
M IV	166	56	−142	420	72.0	78.0	6.1	5.1
IVC-	120	50	−72	245	113	72.5	3.8	2.9
bridge	140	67	−72	146	97.0	82.5	1.9	1.7
	200	50	−72	344	30.0	76.5	5.4	4.1

The results are given in Table 4. We list the name of the complex, the coordinates and velocity V at the sampled position; the initial parameters V_0, α and θ of the fitting test particle; its distance r and altitude z. As can be seen, the fitting requires altitudes $\theta \geq \theta_0 = 72.5°$, (i.e. ejections through the HI-hole), and very large values of V_0.

On the other hand, velocities and coordinates similar to those of the OCCs with $-40 \leq V(\mathrm{km\,s^{-1}}) \leq -20$ at $\bar{b} = +65°$ and $+75°$ in the GQs II and III could be produced with test particles ejected beyond the cutoff value θ_0 with velocities V_0 not larger than about $65\,\mathrm{km\,s^{-1}}$.

6. Discussion of the results. Conclusions

We computed positions, distances, and radial velocities for test particles, which were ejected almost isotropically from a small volume centered at E through the effects of an explosive event. Ballistic orbits were assumed. We adopted a standard solution having $\tau = 35\,Myr$, and E at $r_0 = 121\,\mathrm{pc}$ in the direction $l_0 = 140°$ (Olano 1982), and a mean altitude $z_0 = +35\,\mathrm{pc}$ above the galactic plane. The assumed initial parameters include a cutoff at $\theta_0 = +72.5°$ (cf. Table 1). At low latitudes a large fraction of the observed OCCs can be fitted approximately by our simple standard solution. However, in the GQs I and IV at $\bar{b} = \pm 15°$ the ballistic approximation is not satisfactory and Olano's model 1 makes a better fit. The motions of the fitted OCCs are consistent with an *expansion*. Among the remaining non-fitted OCCs, a significant fraction can be understood as relatively distant objects, which are moving mainly on circular orbits about the galactic center C. At intermediate and high latitudes the ballistic approximation becomes more satisfactory and the fraction of the OCCs fitted by the standard solution increased considerably. Among the fitted OCCs the abundance of negative velocities becomes overwhelming at the high latitudes. The corresponding motions are consistent with a *falling* to the galactic plane.

A significant fraction of the *non-fitted* OCCs belongs to regions, which appear to have been disturbed by the ulterior processes of star formation (e.g. the Sco-Cen shells and the Ori-Eri superbubble). As a check, we considered the effects of three different disturbance centers, each one producing a radial acceleration during a time interval t, which is short, as compared to τ. Their parameters were chosen as to be very roughly consistent with those of the Loop I, the Ori OB1 association, and the Her-shell, respectively (cf. Table 2). The corrections obtained for the test particles were in the sense of *improving* the fit.

Our simple standard solution also fits very roughly the shape of the well-known northern hole in the distribution of the HI of low velocities, by assuming, that it was produced by particles ejected with altitudes $\theta \geq \theta_0$. We suggest that the hole is a signature of the explosion, indicating the *ionization* and *transfer* of gas into the lower halo (cf. Paper I). The resulting interaction could be the origin of the observed northern polar soft X-ray enhancement, which is not related to the North Polar Spur. We quote that the hole is also apparent in the data of Westphalen (1997) regarding the diffuse high-dispersion HI-component detected in the ISM (Kalberla et al. 1998) (cf. Fig. 4). Presumably, this component is very turbulent and extends into the halo. Moreover, samples of the HVC complex M were fitted by assuming test particles ejected beyond the cutoff θ_0 with very high initial velocities. Analogously, the bulk of the OCCs with $-40 \leq V(\mathrm{km\,s^{-1}}) \leq -20$ related to the IVCs at $\bar{b} = +65°$ and $+75°$ in the GQs II and III could be fitted by particles with V_0 not larger than about $65\,\mathrm{km\,s^{-1}}$ and $\theta \geq \theta_0 = 72.5°$.

Our main conclusion is that the global characteristics of the kinematics of the local CNM at $\mid b \mid > 10°$ appear to be *well consistent* with the assumption of an energetic explosive event, of characteristics like those assumed in Olano's models (cf. Table 1).

Acknowledgements. We thank Dr. E. Bajaja for reading the manuscript constructively. We are grateful to the members of the computational staff Messrs. F.A. Bareilles, C. Cristina Miguel and M. Fumagalli, as well as Mrs. N. Perón for their helpful computational assistance. We thank the helpful comments by the referee, Prof. A. Blaauw.

References

Bates, B., Shaw, C.R., Kemp, S.N., Keenan, F.P., 1995, ApJ 444, 672
Blaauw, A., 1965, Koninkl. Ned. Akad. Wetenschap. 74, No. 4
Blaauw, A., 1983, Ir. Astron. J. 16, 141.
Blaauw, A., 1991, in Physics of Star Formation and Early Stellar Evolution, eds. N. Kylafis, and Ch.J. Lada, Kluwer Acad. Pub., p. 125
Brown, A.G.A., de Geus, E.J., de Zeeuw, P.T., 1994, A&A 289, 101
Brown, A.G.A.,Hartmann, D., Burton, W.B., 1995, A&A 300, 903
Chandrasekhar, S., 1942, Principles of Stellar Dynamics, Univ. of Chicago Press
Cohen, M., 1995, ApJ 444, 874
Colomb, F.R., Pöppel, W.G.L., Heiles, C., 1980, A&AS 40, 47
Comerón, F., Torra, J., 1992, A&A 261, 94
Comerón, F., Torra, J., 1994, A&A 281, 35
Dame, T.M., Ungerechts, H.G., Cohen, R.S. et al., 1987, ApJ 322, 706
de Geus, E.J., 1988, Ph.D. thesis, Leiden University
de Geus, E.J., 1992, A&A 262, 258
de Zeeuw, P.T., Hoogerwerf, R., de Bruijne, J.H.J., et al., 1999, AJ 117, 354.

Dickey, J.M.,1993, in: The Minnesota Lectures on the structure and dynamics of the Milky Way, R.M. Humphreys ed., ASP Conference Series, Vol. 39
Franco, J., Tenorio-Tagle, G., Bodenheimer, P., et al., 1988, ApJ 333, 826
Frisch, P.C., York, D.G., 1983, ApJ 271, L59
Gir, B.-Y., Blitz, L., Magnani, L., 1994, ApJ 434, 162
Hartmann, D., Magnani, L., Thaddeus, P., 1998, ApJ 492, 205
Heiles, C., Habing, H.J., 1974, A&AS 14, 1
Herbstmeier, U., Mebold, U., Snowden, S.L., et al., 1995, A&A 298, 606
Houck, J.C., Bregman, J.N., 1990, ApJ 352, 506
Hulsbosch, A.N.M, 1968, Bull. Astr. Inst. Netherlands 20, 33
Ikeuchi, S., 1988, Fund. Cosmic Phys. 12, 225.
Kalberla, P.M.W., Westphalen, G., Mebold, U., et al., 1998, A&A332, L61
Kulkarni, S.R., Fich, M., 1985, ApJ 289, 792
Kulkarni, S.R., Heiles, C., 1987, in: Interstellar Processes, H. Thronson and D. Hollenbach eds., Reidel Pub. Co., p. 87
Kuntz, K.D., Danly, L., 1996, ApJ 457, 703
Lépine, J.R.D., Duvert, G., 1994, A&A 286, 60
Lindblad, P.O, 1967, Bull. Astr. Inst. Netherland 19, 34
Lindblad, P.O., Grape, K., Sandqvist, A. et al., 1973, A&A 24, 309
Lindblad, P.O., Palouš, J., Lodén, K., et al. 1997, Proc. Hipparcos Venice' 97, p. 507
Magnani, L., Hartmann, D., Speck, B.G., 1996, ApJS 106, 447
Meyerdierks, H., 1992, A&A 253, 515
Meyerdierks, H., Heithausen, A., Reif, K., 1991, A&A 245, 247
Minezaki, T., Cohen, M., Kobayashi, Y., et al., 1998, AJ 115, 229.
Ng, Y.K., Bertelli, G., Chiosi, C. et al., 1997, A&A 324, 65
Olano, C.A., 1982, A&A 112, 195
Pöppel, W.G.L., 1997, Fund. Cosmic Phys. 18, 1 (Sect. 4.7 by W.G.L. Pöppel, P. Marronetti and P. Benaglia is Paper II)
Pöppel, W.G.L., Marronetti, P., Benaglia, P., 1994, A&A 287, 601 (Paper I)
Ramesh, B., 1994, J. Astrophys. Astron. 15, 415
Sandqvist, Aa., Lindroos, K.P., 1976 A&A 53, 179
Snowden, S.L., Freyberg, M.J., Plucinsky, P.P. et al., 1995, ApJ 454, 653
Weaver, H., 1979, IAU Symp 60, 573
Wesselius, P.R., Fejes, I., 1973, A&A 24, 15
Westin, T.N.G., 1985, A&AS 60, 99
Westphalen, 1997, Ph.D. Thesis, Univ. of Bonn